Available online at Wisvora

Journal of Global Governance and Sustainability

Journal homepage: https://wisvora.com/index.php/jggs/index

Automation and Sustainability: Developing coating thickness detection algorithm for construction H-shaped steel components

Mu-Chun Su, F.IET [1], Jieh-Haur Chen, F.IET [2*], Wei-Jen Lin [3], Tzuyang Yu [4], and Yu-Jen Chiang [5]

[1]Distinguished Professor, Department of Computer Science and Information Engineering;Dean, College of Electrical Engineering and Computer Science, National Central University, Zhongli, Taoyuan 320317, Taiwan.
[2]Distinguished Professor, Department of Civil Engineering; Director, Research Center of Smart Construction; and Associate Dean, College of Engineering, National Central University, Zhongli, Taoyuan 320317, Taiwan.
[3]PhD Student, Department of Computer Science and Information Engineering, National Central University, Zhongli, Taoyuan 320317, Taiwan.
[4]Professor, Department of Civil and Environmental Engineering; Director, Structural Engineering Research Group (SERG), NDT/SHM Lab, Electromagnetic Remote Sensing Lab; Institutional lead, TIDC at UMass Lowell; University of Massachusetts, Lowell, MA 01854, USA.
[5]Graduate Student, Department of Civil Engineering, National Central University, Zhongli, Taoyuan 320317, Taiwan.

ABSTRACT

To enhance the longevity and sustainability of structural materials, H-shaped steel coated with specialized protective layers has emerged as a superior solution due to its high resistance to rust and fire. However, ensuring the optimal performance and lifecycle efficiency of such materials relies heavily on the precise, automated assessment of coating thickness—an area where traditional detection methods remain error-prone and inefficient. This study addresses the need for a sustainable, automated solution by developing an intelligent detection algorithm based on ResNet, a deep convolutional neural network architecture known for its high performance in visual recognition tasks. A comprehensive dataset of 23,900 annotated images was constructed under a statistically robust sampling strategy, ensuring a 95% confidence level with a 5% margin of error in a balanced 50–50 distribution. Of these, 19,100 images were used to train the CNN model, while 4,800 were reserved for rigorous validation and testing. The dataset was systematically categorized into three distinct coating conditions: uncoated, partially coated, and fully coated. Using a 5-fold cross-validation approach, the proposed model achieved a high accuracy rate of 93%, demonstrating its effectiveness in classifying coating levels. This advancement represents a critical step toward automated, scalable quality control in steel production and infrastructure maintenance. By reducing reliance on manual inspection and minimizing material waste or under-coating, the system contributes to sustainable construction practices and extends the service life of structural steel components.

KEYWORDS

H-shaped steel component, Deep Neural Networks (DNN), pattern recognition, coating, automation, sustainable assessment.

* *Corresponding author: Jieh-Haur Chen* (e-mail: jhchen@ncu.edu.tw)

Received November 17, 2025; Accepted December 16, 2025
Available online December 26, 2025

1. INTRODUCTION

H-shaped steel components find widespread application in building structures, primarily due to their notable advantages in terms of load-bearing capacity and reduced susceptibility to fractures compared to concrete beams and columns, as documented in reference [1]. The shear strength and axial compression performance of these components have undergone comprehensive evaluation in various studies [2-4]. Characterized by their relatively lightweight nature, coupled with surface plasticity and toughness, H-shaped steel components frequently serve as pivotal beam-column elements within structural engineering. They play a crucial role in supporting steel structures, while also finding utility as foundation piles within infrastructure engineering, thereby imparting robustness to building foundations. While the structural merits of H-shaped steel components are evident, the inherent steel material does possess certain limitations, namely, subpar fire resistance [5, 6] and inadequate corrosion resistance [7-9]. This underscores the significance of implementing a fire-resistant and anti-corrosion coating treatment on the surface of H-shaped steel. A well-chosen surface coating treatment can effectively mitigate these shortcomings, leading to enhancements in the longevity and safety of steel structures [10-13]. To predict the fire-resistant performance of such coatings, previous studies have harnessed artificial intelligence and finite element analysis [14, 15]. The coating process necessitates careful consideration of numerous factors, aiming to achieve a balance between cost-effectiveness and optimal results. This involves maximizing product quality while complying with various constraints and governmental regulations. Coating procedures are typically guided by regulatory frameworks established in each respective country. The performance of coated steel is influenced by various factors, including the choice of coating materials, spraying techniques, steel preprocessing, and coating application methods. Different coating materials serve specific purposes in different environments. Moreover, challenges arising from environmental conditions, such as high humidity, uniformity of steel surfaces, spraying equipment, techniques, and potential areas of incomplete coverage, may arise. Prior to applying coatings to H-shaped steel components, necessary preprocessing steps are essential to ensure coating quality, which is often linked to coating thickness [16, 17].

In this study, a cutting-edge coating thickness detection system is devised, harnessing the power of Residual Learning Network (ResNet) bolstered Convolutional Neural Networks (CNN). Digital images are methodically sorted into three distinct categories, each representative of a specific coating scenario: uncoated, partially coated, and fully coated. The system operates through a two-fold process: initial surface coating identification followed by the integration of the identification system into a microcomputer that interfaces with the spraying apparatus. The selected coating constituents serve as a foundational layer to preemptively inhibit the risk of rust formation. Adhering to the established regulations in Taiwan, the stipulated coating thickness requirement surpasses 100 μm, a benchmark diligently adhered to in the course of this research endeavor.

2. H-SHAPED STEEL COATING

The consideration of fire resistance is imperative for the majority of H-steel coatings, even those designed to possess anti-rust properties [6-9]. The composition of coating paints encompasses elements such as zinc, cadmium, aluminum, chromium, nickel, iron oxide, and silver. Coatings incorporating zinc and aluminum ingredients play a pivotal role in averting galvanic corrosion, particularly when two or more dissimilar metals are conjoined [18, 19]. The presence of cadmium within coatings proves effective in mitigating stress cracking corrosion. Notably, intumescent coatings, upon exposure to heat, form a protective insulating layer that shields the steel structure and enhances fire resistance [15]. The proficiency of workers engaged in the coating process significantly influences the durability of the final product. Skilled professionals are tasked with ensuring uniform application to adhere to coating regulations; however, occasional rework or corrective measures may be necessary. Effective training and substantial experience are prerequisites for such industry personnel. The potential of employing robotic devices for coating tasks, controlled and planned along predefined paths, offers an avenue to streamline the process. This approach not only reduces labor costs but also enhances efficiency and the longevity of coatings [20-22]. Many coating criteria center around establishing the minimum coating necessary to satisfy essential safety prerequisites. The regulatory coating standards employed in this study are succinctly outlined in Table 1. However, the existing systems do not

yet possess the capability to quantify coating uniformity, a pivotal factor in determining the quality of H-shaped steel components.

Table 1. Coating regulations

Coating sequence	Coating quantity	Thicknessμm Dry	Wet	Coating interval Min	Max
1 Surface	Grit blasting				
2 Surface	1	50	100	8Hrs	90 Days
3 Top	1	45	100	8Hrs	90 Days

3. APPROACHES TO COATING THICKNESS DETECTION

Recent strides in artificial intelligence and contemporary mathematical techniques have ushered in a fresh wave of methodologies and approaches in the realm of coating detection. Scholars have undertaken comprehensive surveys encompassing metal coating detection and film analysis. A substantial portion of these methods has been introduced by researchers specializing in machine learning and sensor technology [23, 24]. Within this domain, researchers have devised a high-precision approach to detect dust deposition, involving numerical simulations to gauge coating thickness in ventilation and dust collection conduits. The toolkit of instrumental techniques includes X-ray micro-chromatography, guided ultrasonic wave testing, and terahertz pulsed imaging sensors, all in tandem with mathematical methodologies [25-30].

In parallel studies, ice thickness has been gauged through the principles of light refraction, employing algorithms such as fast Fourier transformation, image processing, and machine vision [31-33]. A gamut of classification algorithms comes into play, encompassing logistic regression, Naïve Bayes, k-nearest neighbor, as well as decision tree, random forest, and support vector machine methodologies. These algorithms introduce frameworks for data classification tailored to specific applications. For instance, the logistic regression algorithm, rooted in linear regression, applies the sigmoid function to classify data into distinct groups [34]. Operating on the presumption of independent features, the probability distribution, derived by multiplying all conditional probabilities, exhibits predictive/classification capabilities [35]. In the k-nearest neighbor algorithm, the Euclidean distance, Manhattan distance, or Minkowski distance quantifies the separation between new and preexisting data. The algorithm designates k preexisting data points as selection criteria, with the shortest k data points serving as the boundary. Given potential differing labels at the boundary, the new data is classified into the group with the most frequent occurrence label within the boundary [36, 37]. Decision tree methodologies derive classification rules from the distinct attributes/features of each dataset. This genre encompasses algorithms like ID3, C4.5, CART, SLIQ, and SPRINT [38, 39].

Natural language processing relies on widely used algorithms like long short-term memory and recurrent neural networks [40]. In the spheres of image and audio processing, requisites include image recognition, machine vision, and speech-to-text translation. Intel's OpenCV tool serves as a versatile solution for a multitude of image processing tasks. In audio processing, activities range from dynamic range compression/expansion to equalizing signals with diverse frequencies and confining signals within specific threshold ranges [41]. In the realm of robotics, the fusion of automatic control systems and machine vision emerges as a recurring theme, enhancing the capabilities and functionalities of these systems. Machine learning endows computers with the ability to execute tasks sans explicit programming or instruction, constituting a pivotal facet within the broader domain of artificial intelligence.

In recent times, the utilization of deep convolutional neural networks (CNNs) has become prevalent for discerning features within images and videos [42, 43]. Foundational elements within deep convolutional neural networks encompass convolution layers [44], activation layers [33, 45], pooling layers [46], and fully connected layers [47]. An outline of the typical functioning of a CNN is as follows: Input data is divided into smaller segments to extract features, which are then subjected to convolution with weights, bias, kernels, or filter passes to span the entire image. Outputs that traverse the pooling layer are obtained, with three types of pooling in play: max pooling, min pooling, and average pooling. This pooling layer amalgamates neighboring information, determining values, thereby progressively reducing data dimensions. Frequently employed activation functions encompass Relu, Sigmoid, and Adam. Through iterations of the aforementioned processes, the eventual output emerges as the classification result. A conclusive classification function, like SoftMax, establishes the probability associated with a particular class.

4. DATA COLLECTION

The digital images utilized in this study were gathered through a convenient sampling approach within the field of coating. This field corresponds to the largest coating site for construction H-shaped steel in northern Taiwan, constituting approximately one-third of the total volumes within the country. To adhere to the sampling criteria necessitating 95% confidence and a 5% margin of error within the 50–50 category [48, 49], a total of 23,900 images were conveniently selected. The image collection process was seamless, requiring only a few days. A comprehensive breakdown of the collected images is provided in Table 2. Out of these, 19,100 images were chosen at random for the training of the CNN networks, while the remaining 4,800 images were reserved for evaluation and testing purposes. An illustrative example of these images is depicted in Figure 1, with each image boasting dimensions of 3,000 by 3,000 pixels. To augment the dataset, every image was partitioned into multiple smaller segments of 224 by 224 pixels, serving as input data for the proposed CNN. This augmentation strategy serves a dual purpose: it not only amplifies the dataset but also contributes to the establishment of a more accurate model. Additionally, the data undergoes random transformations such as rotation, zooming, and the introduction of Gaussian noise. To ensure robustness, all images were allocated into training and testing sets through a 5-fold cross-validation approach.

Table 2. Data distribution

	Number of training data	**Number of testing data**
Uncoated	2,900	500
Partial coated	11,800	2,900
Fully coated	4,400	1,400
Total	19,100	4,800

Figure 1. Sample image for coating detection

5. PROPOSED METHOD AND RESULTS

The algorithm's inception entails the meticulous selection and configuration of parameters, encompassing the choice of loss function, optimizer, learning rate, epochs, batch size, and classification function, as illustrated in Figure 2. In the context of machine learning, the loss function serves as a metric to quantify the disparity between predicted output and labeled output, with the goal of minimizing this difference to enhance accuracy. For classification tasks, the widely adopted loss function is cross-entropy, particularly binary cross-entropy when dealing with two distinct groups. In the context of this study, data is classified into either five or three groups, rendering categorical cross-entropy the most apt choice as the loss function. Cross-entropy, in essence, quantifies the dissimilarity between probability distributions. Specifically, categorical cross-entropy caters to scenarios where data is partitioned into multiple classes, ensuring that each data point is exclusively associated with a single class. The mathematical representation of the loss calculation is expressed by Equation (1):

$$loss = -\sum_{i}^{number\ of\ classes} t_i \cdot log\ (p_i) \quad (1)$$

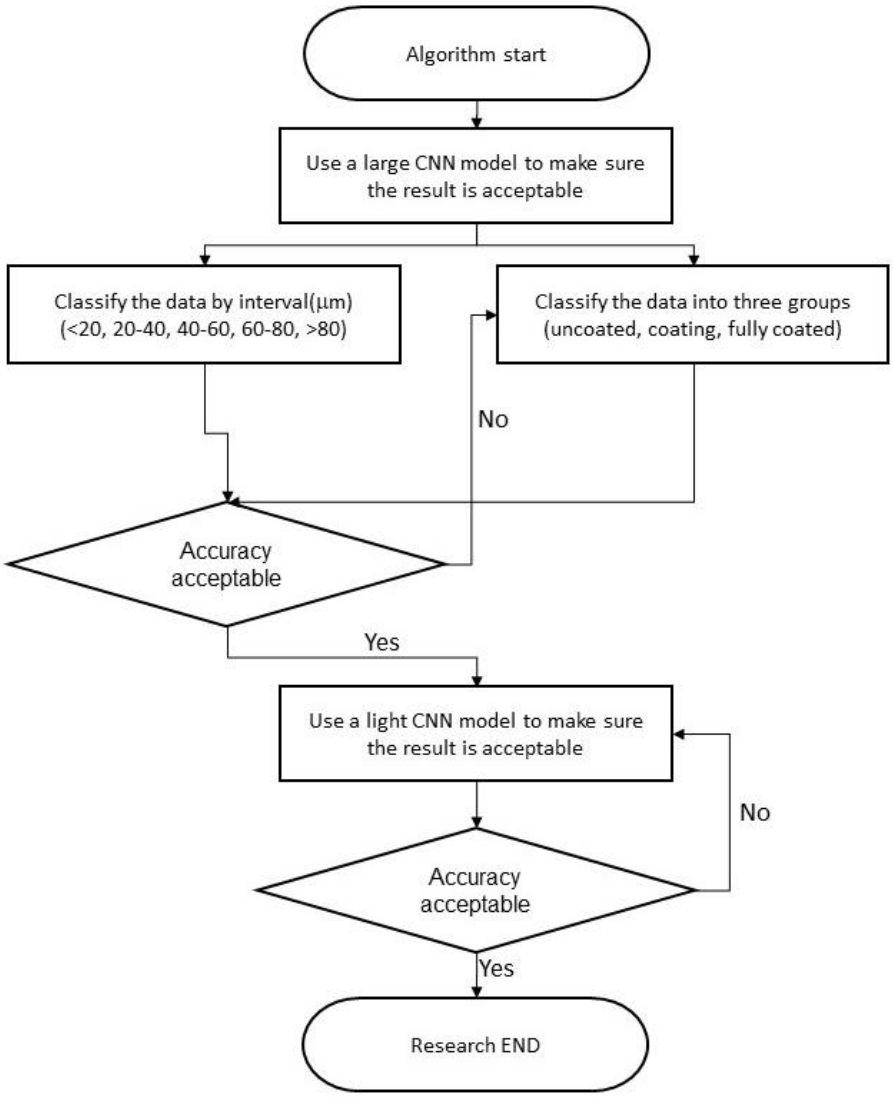

Figure 2. Algorithm design flow

where *i* represents the amount of data, it is the target value of the i^{th} data, and p_i is the predicted output of i^{th} data. The cross entropy is positive as long as target is not equal to the predicted value.

An optimizer is a pivotal algorithm tasked with fine-tuning parameters to minimize loss and enhance accuracy. Among the fundamental and widely embraced optimizers is stochastic gradient descent (SGD). This technique refines weights by augmenting prior weights with the product of the learning rate and weight gradient. Introducing directional velocity in this process propels optimization, expediting convergence while mitigating oscillation when training veers off course:

$$SGD: W \leftarrow W - \alpha \frac{\partial L}{\partial W} \quad (2)$$

$$Momentum: V(t) \leftarrow V(t) - [\gamma V(t-1) + \alpha \frac{\partial L}{\partial W}] \quad (3)$$

where the gradient computation involves determining the partial derivative of the loss function concerning the weight parameter. In this context, α signifies the learning rate of the model, serving as the stride for weight updates. Meanwhile, γ constitutes a constant, typically assigned a value like 0.9 or an analogous figure in the momentum optimizer.

The Adam optimizer, which amalgamates stochastic gradient descent and momentum, aligns with the aforementioned requirements and is adopted for this study. In this approach, the learning rate is dynamically adjusted based on the root mean square of prior gradients at each step. This mechanism enhances both learning accuracy and efficiency, addressing challenges such as overshooting the minimum with a high learning rate or inefficiency arising from a low learning rate. Adam is a

favored choice for optimization in the machine learning realm, as advocated by multiple models within the field (Oshiro et al., 2012). Notably, Adam continually refines the learning rate throughout the iterative process:

$$m_t = \beta_1 m_{t-1} + (1-\beta_1)\frac{\partial L_t}{\partial W_t} \tag{4}$$

$$v_t = \beta_1 v_{t-1} + (1-\beta_2)(\frac{\partial L_t}{\partial W_t})^2 \tag{5}$$

$$\widehat{m}_t = \frac{m_t}{1-\beta_1^t} \tag{6}$$

$$\widehat{v}_t = \frac{v_t}{1-\beta_2^t} \tag{7}$$

$$Adam: W \leftarrow W - \alpha\frac{\widehat{m}_t}{\sqrt{\widehat{v}_t}+\varepsilon} \tag{8}$$

Adam retains not only the exponentially decaying average of past squared gradients (β1), which effectively addresses the issue of drastic learning rate decay, but also maintains an exponentially decaying average of past gradients (β2). Biased-correction is implemented through Equations (6) and (7) for the first and second moment estimates, respectively. The parameter β1 is conventionally assigned a value of 0.9,

β 2 is set to 0.999, and ε is set to $10e^{-8}$.

Regarding the remaining parameter configurations, which encompass the output activation function, number of epochs, and batch size, the dense layer is employed. Additionally, the flattening process is directly employed to transform the 3D feature maps (encompassing width, height, and channels) into a singular dimension (width*height*channels). This dense layer, alternatively known as the fully connected layer, computes the dot product of kernels and input data, incorporating a bias term. Subsequently, the outcome of this calculation is subjected to the activation function—specifically, the SoftMax function—thus culminating in the establishment of the classification outcome, as depicted in the ensuing equation:

$$output = \frac{e^{z_i}}{\sum_{i=1}^{n} e^{z_i}} \tag{9}$$

where *n* represents the group number, either 3 or 5 in this study.

The number of epochs often goes hand in hand with the batch size, which dictates the quantity of data processed before parameter updates occur. A smaller number of epochs generally results in well-trained parameters but lower accuracy. Conversely, a larger number of epochs can significantly prolong computation time. Setting the batch size too small, say to one, can potentially lead to overfitting and training complications. Thus, the choice of batch size is frequently influenced by computational efficiency. In the context of this study, the batch size and epoch count were fine-tuned through iterative experimentation to achieve an acceptable accuracy level (> 90%) while employing ResNet and MobilenetV2 applications. The parameter configurations for both applications are outlined in Table 3.

Table 3. Parameter settings

Parameters	**ResNet**	**MobileNetV2**
Image size	(224,224,3)	(224,224,3)
Loss function	Categorical cross entropy	Categorical cross entropy
Optimizer	Adam	Adam
Learning rate	0.0001	0.0001
Batch size	8	32
Epoch	200	200

The outcome comparison between the two applications is depicted in Table 4, revealing a marginal advantage in favor of the ResNet-enhanced CNN with a 93% accuracy rate. The predictive accuracies showcased in Table 4 comfortably exceed the 90% threshold, underscoring their practical viability. Figures 3 and 4 showcase the testing accuracies for ResNet and MobileNetV2, revealing a slight tendency toward overfitting in the training results during model training. Confusion matrices for ResNet and MobileNetV2 are detailed in Tables 5-8, elucidating the occurrence attributed to data disparities. This can be attributed to the labeling of data, which is determined through averaging across nine points of coating. Given the inherent variations in coating across different points due to the manual application process, some degree of inaccuracy (7%) might manifest in the classification output. However, despite this, the model's overall accuracy remains practical for coating operations involving construction H-shaped steel components.

Table 4. Result comparison

Model Name	Model Size (MB)	Model Accuracy ImageNet	Layers	Parameters
ResNet152	232	0.931	152	60,419,944
MobileNetV2	14	0.901	53	3,538,984

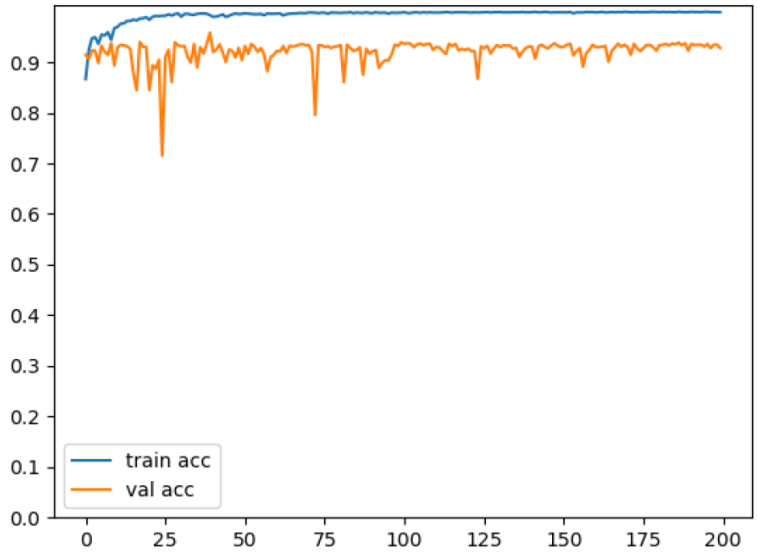

Figure 3. Accuracy by ResNet

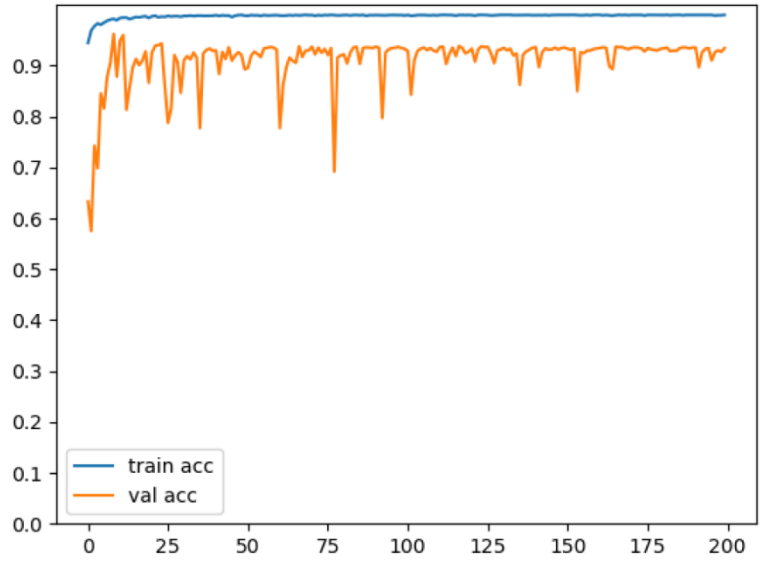

Figure 4. Accuracy by MobileNetV2

Table 5. Confusion matrix for ResNet

	Uncoated	Partial coated	Fully coated
Fully coated	1057	3	340
Uncoated	0	500	0
Partial coated	2	0	2898

Table 6. Confusion matrix for MobileNetV2

	Uncoated	Partial coated	Fully coated
Fully coated	1089	0	311
Uncoated	0	500	0
Partial coated	0	3	2897

Table 7. Classification report for ResNet

	Precision	Recall	F1-score	Support
Fully coated	1.00	0.76	0.86	1400
Uncoated	0.99	1.00	1.00	500
Coating	0.89	1.00	0.94	2900
Accuracy	0.93			4800
Macro acc	0.96	0.92	0.93	4800
Weighted acc	0.94	0.93	0.93	4800

Table 8. Classification report for MobileNetV2 (three processes)

	Precision	Recall	F1-score	Support
Fully coated	1.00	0.78	0.88	1400
Uncoated	0.99	1.00	1.00	500
Coating	0.90	1.00	0.95	2900
Accuracy	0.93			4800
Macro acc	0.97	0.93	0.94	4800
Weighted acc	0.94	0.93	0.93	4800

6. CONCLUSION

The existing manual coating processes face substantial challenges and limitations within current industries. A key challenge stems from a pronounced scarcity of skilled workers, while a notable limitation persists in the form of inconsistent coating practices for construction H-shaped steel components. In response, this study is dedicated to addressing these issues through the development of a dedicated coating detection algorithm tailored for construction H-shaped steel components. Employing a sampling framework rooted in 95% confidence and a 5% margin of error within the 50-50 category, a comprehensive dataset of 23,900 images was thoughtfully collected. Subsequent phases encompassed algorithm formulation and evaluation, wherein a subset of 19,100 randomly selected images was allocated for training CNN networks, while the remaining 4,800 images were reserved for evaluation and testing. The outcome of the ResNet-enhanced CNN algorithm yielded an impressive accuracy rate of 93%.

The novel contribution of this research lies in the innovative algorithm meticulously designed to address coating issues, thereby mitigating the risks associated with uncoated or partially coated construction H-shaped steel components. As a result, the practical implementation of automated coating detection becomes a feasible proposition for the industry. Future investigations may explore the integration of this algorithm with industrial robots and depth sensors to automate coating processes. It's important to note that while the study focuses on bottom painting, primarily in red, the algorithm's potential applicability to coatings of other colors is also noteworthy. Moreover, the algorithm's utility could extend to various construction materials necessitating coating. Further experimentation is warranted to thoroughly assess its feasibility and effectiveness.

DATA AVAILABILITY STATEMENT

All data, models, and the code generated or used during the study appear in the submitted article.

ACKNOWLEDGMENTS

The authors extend their gratitude for the partially support provided for this research by the Taiwan Ministry of Science and Technology (MOST) / National Science and Technology Council (NSTC) under the grant numbers MOST-108-2221-E-008 -002 -MY3, MOST-109-2622-E-008 -018 -CC2, MOST- 110-2622-E-008 -018 -CC2, MOST-110-2221-E-008 -052 -MY3, NSTC-111-2622-E-008-017, and NSTC-111-2221-E-008 -027 -MY3. It is important to note that any opinions, findings, conclusions, and recommendations presented in this paper solely belong to the authors and do not necessarily reflect the perspectives of the MOST/NSTC.

CONFLICT OF INTERESTS

The authors declare that they have no known competing financial interests or personal relationships that could have appeared to influence the work reported in this paper.

REFERENCES

[1] Zheng, H., Z. Chen, and J. Xu (2016). "Bond behavior of H-shaped steel embedded in recycled aggregate concrete under push-out loads." *International Journal of Steel Structures*, 16(2), 347-360.

[2] Nie, J.-G., et al. (2013). "Shear strength of trapezoidal corrugated steel webs." *Journal of Constructional Steel Research*, 85, 105-115.

[3] Shang, H., et al. (2019). "Experimental studies on shear resistance performances for the shear key of H shape steel spatial grid roofs." *Latin American Journal of Solids and Structures*, 16(5), 1-17.

[4] Wang, Y.-B., et al. (2012). "Experimental and numerical study on the behavior of axially compressed high strength steel columns with H-section." *Engineering Structures*, 43, 149-159.

[5] Kucukler, M., Z. Xing, and L. Gardner (2020). "Behaviour and design of stainless steel I-section columns in fire." *Journal of Constructional Steel Research*, 165, 105890.

[6] Reis, A., N. Lopes, and P. Real (2019). "Ultimate shear strength of steel plate girders at normal and fire conditions." *Thin-Walled Structures*, 137, 318-330.

[7] Angst, U. (2018). "Challenges and opportunities in corrosion of steel in concrete." *Materials and Structures*, 51(1), 1-20.

[8] Dwivedi, D., K. Lepková, and T. Becker (2017). "Carbon steel corrosion: a review of key surface properties and characterization methods." *RSC Advances*, 7(8), 4580-4610.

[9] Poursaee, A. (2016). "Corrosion of steel in concrete structures." *Corrosion of steel in concrete structures*, 19-33.

[10] Itoh, Y., et al. (2013). "Anticorrosive performance of repair painting as remedy for deterioration in metallised steel." *Corrosion Engineering, Science and Technology*, 48(7), 537-551.

[11] Lyon, S., R. Bingham, and D. Mills (2017). "Advances in corrosion protection by organic coatings: What we know and what we would like to know." *Progress in Organic Coatings*, 102, 2-7.

[12] Mills, D. and S. Jamali (2017). "The best tests for anti-corrosive paints. And why: A personal viewpoint." *Progress in Organic Coatings*, 102, 8-17.

[13] Thierry, D., et al. (2011). "Corrosion protection and corrosion mechanisms of continuous galvanised steel sheet with focus on new coating alloys." *Proc. Galvatech 8th International Conference on Zinc and Zinc Alloy Coated Steel Sheet, Genova, Italy*.

[14] Arabasadi, Z., et al. (2013). "Prediction and optimization of fireproofing properties of intumescent flame retardant coatings using artificial intelligence techniques." *Fire Safety Journal*, 61, 193-199.

[15] Zakwan, F., et al. (2020). "Finite Element Analysis of Coated (Intumescent Coating Protection) Cellular Steel Beam (CSB) Expose to Fire." 012032.

[16] Jamali, S. and D. Mills (2014). "Steel surface preparation prior to painting and its impact on protective performance of organic coating." *Progress in Organic Coatings*, 77(12), 2091-2099.

[17] Standard, N. (2012). "Surface preparation and protective coating." *NORSOK M-501*, Norway.

[18] Mousavifard, S., et al. (2013). "The effects of zinc aluminum phosphate (ZPA) and zinc aluminum polyphosphate (ZAPP) mixtures on corrosion inhibition performance of epoxy/polyamide coating." *Journal of Industrial and Engineering Chemistry*, 19(3), 1031-1039.

[19] Naderi, R. and M. Attar (2010). "The role of zinc aluminum phosphate anticorrosive pigment in protective performance and cathodic disbondment of epoxy coating." *Corrosion Science*, 52(4), 1291-1296.

[20] Cai, Z., et al. (2015). "Computer-aided robot trajectory auto-generation strategy in thermal spraying." *Journal of Thermal Spray Technology*, 24(7), 1235-1245.

[21] Chidhambara, K. and B. Shankar (2018). "Optimization of robotic spray painting process parameters using Taguchi

method." 012108.

[22] Kim, W., et al. (2016). "Development of Auto-spray system to improve the quality of 3D Scanning Quality." *Journal of the Korea Academia-Industrial Cooperation Society*, 17(4), 100-105.

[23] Benoit, M., et al. (2016). "Comparison of different methods for measuring the passive film thickness on metals." *Electrochimica Acta*, 201, 340-347.

[24] Giurlani, W., et al. (2020). "Measuring the thickness of metal coatings: a review of the methods." *Coatings*, 10(12), 1211.

[25] Alves-Lima, D., et al. (2020). "Review of terahertz pulsed imaging for pharmaceutical film coating analysis." *Sensors*, 20(5), 1441.

[26] Olisa, S., M. Khan, and A. Starr (2021). "Review of current guided wave ultrasonic testing (GWUT) limitations and future directions." *Sensors*, 21(3), 811.

[27] Russe, I.-S., et al. (2012). "Validation of terahertz coating thickness measurements using X-ray microtomography." *Molecular Pharmaceutics*, 9(12), 3551-3559.

[28] Wang, H.-C., A. Zyuzin, and A. Mamishev (2013). "Measurement of coating thickness and loading using concentric fringing electric field sensors." *IEEE Sensors Journal*, 14(1), 68-78.

[29] Xu, C., et al. (2020). "A novel high-frequency ultrasonic approach for evaluation of homogeneity and measurement of sprayed coating thickness." *Coatings*, 10(7), 676.

[30] Zhao, Z., G. Liu, and D. Li (2019). "Deposition Thickness Detection Method based on Dust Distribution Law of Ventilation Dust Removal Pipeline." *Proc. 2nd International Conference on Safety Produce Informatization (IICSPI)*, IEEE, 252-256.

[31] Bai, X., et al. (2020). "A Layer Tracking Method for Ice Thickness Detection Based on GPR Mounted on the UAV." *Proc. 4th International Conference on Imaging, Signal Processing and Communications (ICISPC)*, IEEE, 24-28.

[32] Shan, M., et al. (2020). "Deep-learning-enhanced ice thickness measurement using Raman scattering." *Optics Express*, 28(1), 48-56.

[33] Wang, Y., et al. (2020). "The influence of the activation function in a convolution neural network model of facial expression recognition." *Applied Sciences*, 10(5), 1897.

[34] Sperandei, S. (2014). "Understanding logistic regression analysis." *Biochemia Medica*, 24(1), 12-18.

[35] Calders, T. and S. Verwer (2010). "Three naive bayes approaches for discrimination-free classification." *Data Mining and Knowledge Discovery*, 21(2), 277-292.

[36] García-Pedrajas, N., J. Del Castillo, and G. Cerruela-García (2015). "A proposal for local values for k nearest neighbor rule." *IEEE Transactions on Neural Networks and Learning Systems*, 28(2), 470-475.

[37] Zhang, J., et al. (2015). "Precision measurement of coating thickness on ferromagnetic tube using pulsed eddy current technique." *International Journal of Precision Engineering and Manufacturing*, 16(8), 1723-1728.

[38] Brijain, M., et al. (2014). "A survey on decision tree algorithm for classification." *International Journal of Engineering Development and Research*, 1-5.

[39] Oshiro, T., P. Perez, and J. Baranauskas (2012). "How many trees in a random forest?" *Proc. International Workshop on Machine Learning and Data Mining in Pattern Recognition*, Springer, 154-168.

[40] Hirschberg, J. and C. Manning (2015). "Advances in natural language processing." *Science*, 349(6245), 261-266.

[41] Nadkarni, P., L. Ohno-Machado, and W. Chapman (2011). "Natural language processing: an introduction." *Journal of the American Medical Informatics Association*, 18(5), 544-551.

[42] Albawi, S., T. Mohammed, and S. Al-Zawi (2017). "Understanding of a convolutional neural network." *Proc. International Conference on Engineering and Technology (ICET)*, IEEE, 1-6.

[43] Khan, A., et al. (2020). "A survey of the recent architectures of deep convolutional neural networks." *Artificial Intelligence Review*, 53(8), 5455-5516.

[44] Dumoulin, V. and F. Visin (2016). *A guide to convolution arithmetic for deep learning*.

[45] Sharma, S., S. Sharma, and A. Athaiya (2017). "Activation functions in neural networks." (12, 6).

[46] Sun, M., et al. (2017). "Learning pooling for convolutional neural network." *Neurocomputing*, 224, 96-104.

[47] Schwing, A. and R. Urtasun (2015). *Fully connected deep structured networks*.

[48] Chen, J.-H., et al. (2020). "The willingness to adopt the Internet of Things (IoT) conception in Taiwan's construction industry." *Journal of Civil Engineering and Management*, 26, 534–550.

[49] Wang, H.-H., et al. (2022). "Exploring empirical rules for construction accident prevention based on unsafe behaviors." *Sustainability*, 14, 4058.